AD

TR-1383

IMPACT TESTING USING A FOUR-INCH AIR GUN AND LEAD TARGETS

by

Harry J. Davis

April 1968

The findings in this report are not to be construed as an official Department of the Army position, unless so designated by other authorized documents.

Destroy this report when it is no longer needed. Do not return it to the originator.

AD

TR-1383

IMPACT TESTING USING A FOUR-INCH AIR GUN AND LEAD TARGETS

by

Harry J. Davis

April 1968

1

C O N T E N T S

A P P E N D I C E S

I L L U S T R A T I O N S

ILLUSTRATIONS—Cont'd

Page No.

TABLES

4

NOMENCLATURE

a	=	Acceleration
a_0	=	Sonic velocity of gas
A	=	Barrel or projectile base area
b	=	Constant appearing in velocity dependent force law—equation (7)
D	=	Projectile diameter
g	=	Acceleration due to gravity
G_{pk}	=	Peak acceleration expressed in multiples of g
H_T	=	Dynamic hardness of target material
k_0	=	Shape factor of projectile's head (= .5 for sphere).
ℓ	=	Length of projectile
L	=	Length of barrel
m	=	Projectile mass
p	=	Dynamic flow pressure of target material or driving pressure of gas
p_0	=	Initial driving pressure of gas
t_M	=	Duration of penetration process
t_n	=	Natural period of accelerometer
T	=	Target thickness
U_0	=	v/a_0
v	=	Instantaneous projectile velocity
v_0	=	Projectile muzzle velocity
w	=	Projectile weight
x	=	Target penetration depth
x_M	=	Maximum target penetration
α, β	=	Constant appearing in Pencelet law—eq (3)
γ	=	Ratio of specific heat of gases
ρ_p, ρ_T	=	Density of projectile and target material

ABSTRACT

Fuzes and fuze components are tested for ruggedness at the Harry Diamond Laboratories by mounting them in projectiles and firing them from an air gun into lead blocks. This report is an evaluation of this method of testing based upon three years of routine data. The air gun is 96 ft long and has a 4-in. bore. The projectile is 11 in. long, is round nosed, and weighs 17.5 lb with a standard fuze cargo. The muzzle velocity ranges from 100 to 650 fps. The target consists of 3 to 10 in. of lead plates. The projectile deceleration upon striking this target provides the test.

The measured quantity of primary interest is the peak acceleration obtained from copper ball accelerometers. These measurements indicate that structures or components with natural frequencies of hundreds of Hertz experience peak accelerations of 5000 to 50,000 g. However, hundreds of thousands of g's have been measured at natural frequencies greater than 10 kHz. Such measurements may differ by factors of two at different points within the projectile. The advantages and disadvantages of copper ball accelerometers are presented.

The air-gun design and test techniques are discussed briefly. Target penetration phenomena are also discussed, since they provide the force pulses experienced by the projectile. The usual constant retarding force law and the Poncelet solid penetration law are applied to the present study.

1. INTRODUCTION

The modern ordnance fuze is so complex that its dynamic response to impacts cannot be exactly specified by theoretical analysis. A fuze is subjected to accelerations during shipment and while being fired; its dynamic behavior must therefore be determined experimentally before it can be treated as a reliable part of a weapons system. These laboratories have used air-gun techniques to shoot heavy projectiles containing fuzes into lead targets, resulting in high decelerations that may cause structural failures within the fuze. These deficiencies are corrected before the fuze is field tested. This paper examines the phenomena occurring during the lead impact in order to evaluate the shock testing performed.

2. EXPERIMENTAL APPARATUS AND TECHNIQUE

In an HDL ruggedness test, the shell containing the fuze is placed in the breech of the air gun, which is 96 ft long with a 4-in. bore. A tank is filled with air at pressures ranging from 2 to 125 psig which are necessary to achieve the desired projectile velocity

of 100 to 650 fps. A solenoid-operated valve connecting the gun to the tank is opened and the shell is fired through the tube. At initial pressures, ≤ 10 psig, appreciable gas leakage occurs about the projectile as it travels down the tube. To lessen erratic results, a metal disc with a 1-in. hole is inserted in the breech up-stream of the shell. The disc acts as a gas-metering device. Data gathered under these conditions are not discussed in this report. Further details of the gun are given in reference 1.

After leaving the gun the shell travels approximately 5 ft and hits a stack of 6- by 8- by 1-in. lead blocks, which deform plastically while decelerating the shell. This constitutes the impact test. When setting up the test, newly cast blocks are pressed together by hand; no attempt is made to fasten them down. The nose of the shell is usually greased or oiled to ease removal from the lead.

A typical projectile is 4 in. in diameter, 11 in. long, weighs 16.3 lb without fuze cargo, and is made of 4140 steel. The projectile consists of three sections that are screwed together—the nose, cargo section, and end cap (fig. 1). The hemispheric nose constitutes approximately half the total weight of the projectile. The nose shown in figure 1 has a 2-in. radius. Cone-shaped and flattened noses have been used, but will not be discussed here because of insufficient test data. The threaded cargo-carrying portion of the vehicle is an integral part of the 3/16-in. thick walls of the cargo or test-specimen section.

The measurements routinely made in the course of a run are listed in table I, together with an estimate of their accuracy. Experimental data gathered over a period of years were fitted to the function

$$X = cY^p,$$

where suitable pairs of quantities listed in table I can be substituted for X and Y. Some of the resulting relations are used in this paper, whereas others are only of general interest in air-gun design work. Details of the fitting technique and its results are given in appendix A and in tables II(a) and II(b).

Several laws are described in the literature in connection with penetration mechanics. The impact speed and penetration depth data gathered in HDL air-gun testing were fitted, using a least squares technique to the expression predicted by some of these laws. The results (appx B) bear on the evaluation of the 4-in. air-gun test and yield data basic to studies of penetration phenomena.

8

Lead target blocks

Nose

Test specimen section

Copper ball accelerometer

Fuze

Cap
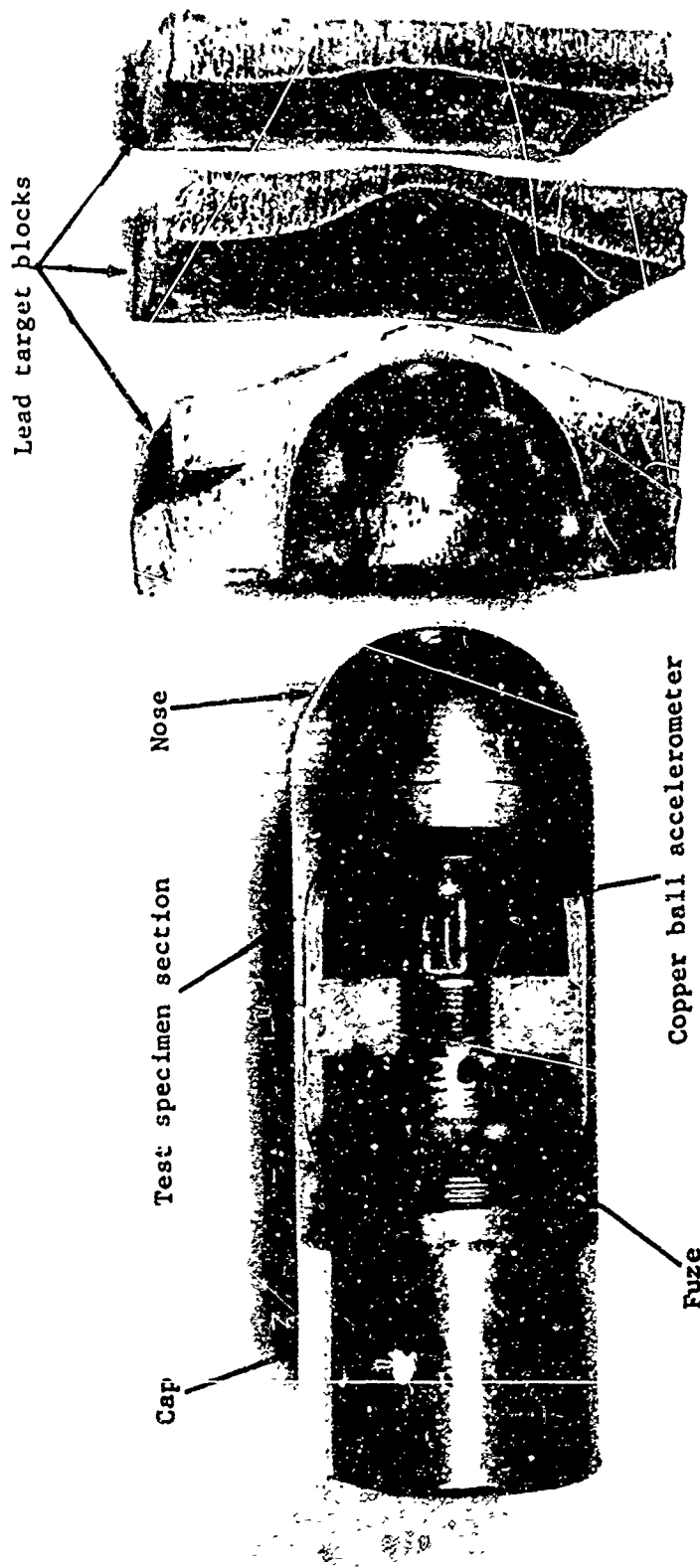
1032-66

Figure 1. Projectile and target blocks used in HDL 4-in. air gun.

Table I. Air-Gun Measurements

Quantity	Estimated accuracy	Remarks
Projectile weight	±1/4 lb	Weight estimate usually made by gun operator
Initial gas pressure	±2 psi	Bourdon tube gage
Projectile muzzle velocity	±1 percent	Light screen technique described in reference 1
Peak deceleration force	Unknown	Mod 1 copper ball accelerometer described in reference 2
Peak penetration depth	±1/4 in.	Machinist's scale inserted in crater. Accuracy is better in shallow penetrations.

Table II(a). Empirical Fit of Air-Gun Data to Equation of Form $X = cY^p$

Data accummulated with accelerometers of natural period t_n where

$w = 17.5$ lb		$t_n = 460$ μsec			$t_n = 340$ μsec			$t_n = 270$ μsec		
X	Y	c	p	σ_p	c	p	σ_p	c	p	σ_p
v_o	p	6.064×10^1	0.478	0.55×10^{-2}	1.183×10^2	0.316	1.1×10^{-2}	7.17×10^1	0.435	0.7×10^{-2}
G_{pk}	p	1.22×10^3	0.685	2.7×10^{-2}	1.124×10^4	0.206	3.5×10^{-2}	1.600×10^3	0.744	4.2×10^{-2}
G_{pk}	v_o	3.678	1.421	5.4×10^{-2}	2.263×10^2	0.782	9.1×10^{-2}	1.263	1.684	9.6×10^{-2}
X_m	v_o	6.4×10^{-4}	1.458	2.7×10^{-2}	8.4×10^{-4}	1.414	4.0×10^{-2}	7.86×10^{-3}	1.054	3.9×10^{-2}
G_{pk}	X_m	5.303×10^3	0.886	3.78×10^{-2}	1.436×10^4	0.400	6.0×10^{-2}	3.956×10^3	1.422	3.2×10^{-2}
Velocity range (fps)		250 - 467			355 - 505			370 - 630		
No. or points		336			310			88		

11

Table II(b). Empirical Fit of Air-Gun Data to Equation of Form
$X = cY^p$

w = 17.5 lb   Shallow Penetration $(x_m \leq \frac{D}{2})$

| X | Y | $t_n = 460$ µsec | | σ_p |
		c	p	
v_o	p	3.902×10^1	0.625	4.0×10^{-2}
G_{pk}	p	1.631×10^3	0.610	5.5×10^{-2}
G_{pk}	v_o	3.791×10^1	1.012	4.3×10^{-2}
X_M	v_o	1.656×10^{-3}	1.267	4.5×10^{-2}
G_{pk}	X_M	6.345×10^3	0.738	4.1×10^{-2}

| Velocity range(fps) | | 81 - 276 | | |

| No. of points | | 68 | | |

w = 23.0 lb $t_n = 340$ usec

X	Y	c	p	σ_p
v_o	p	5.017×10^1	0.491	1.4×10^{-3}
G_{pk}	p	3.517×10^6	0.451	6.6×10^{-3}
G_{pk}	v_o	1.112×10^3	0.893	1.3×10^{-1}
X_M	v_o	1.821×10^{-4}	1.705	8.6×10^{-2}
G_{pk}	X_M	$1.036 \times 10^*$	0.502	7.2×10^{-2}

| Velocity range (fps) | | 267 - 422 | | |

| No. of points | | 52 | | |

The dependence of the shell velocity upon the pressure of the driving gas is important in the design and operation of air guns. The experimental results of this investigation are therefore compared with theoretical predictions in appendix C.

Much of the work described herein depends upon copper ball accelerometers, the characteristics of which are reviewed in appendix D.

3. FORCES ACTING ON THE PROJECTILE AND TEST SPECIMEN

The peak-g impact-velocity fit described in appendix A for 17.5-lb projectiles is plotted in figure 2 for the three different Model 1 copper ball accelerometers used in this work. It can be seen that there are three distinct curves (solid lines), although the reading of any one accelerometer is often interpreted as being indicative of the peak force acting upon the system. The 95-percent confidence limits are also shown in figure 2 by the broken lines. The broad range indicated by the confidence limits is due to variations in the test conditions and to the inaccuracy of the copper ball accelerometer measurements. As discussed in appendix D, copper ball accelerometers approximate a spring-mass system whose response depends upon the ratio of the natural period of the system and a characteristic time that is usually the input-pulse duration. In this study, the copper ball accelerometer does not measure the peak of the driving force but measures the accelerometer response to this force as a function of the accelerometer's natural period. This is the basic characteristic of a shock spectrum (ref 2). The data presented here are therefore the shock spectrum of the system. The copper ball accelerometer may also be considered a test specimen whose response is known, at least to the limits described in appendix D.

A Model 8 copper ball accelerometer (ref 2) obtained from the U.S. Naval Ordnance Laboratory was used to investigate the response further. This device consists of nine copper balls and masses, each mass being different. This provides a group of peak-reading accelerometers with natural periods ranging from 67.5 to 295 μsec, that is, natural frequencies from about 15,000 to 3400 Hz. Runs at different velocities were made using the Model 8 accelerometer; the results for each are shown in figure 3, where peak accelerations are plotted against the natural period and frequency of the accelerometer. The projectile weighed 17.0 lb. Also shown are the results of curve fitting listed in table II determined from the Model 1 accelerometer data.
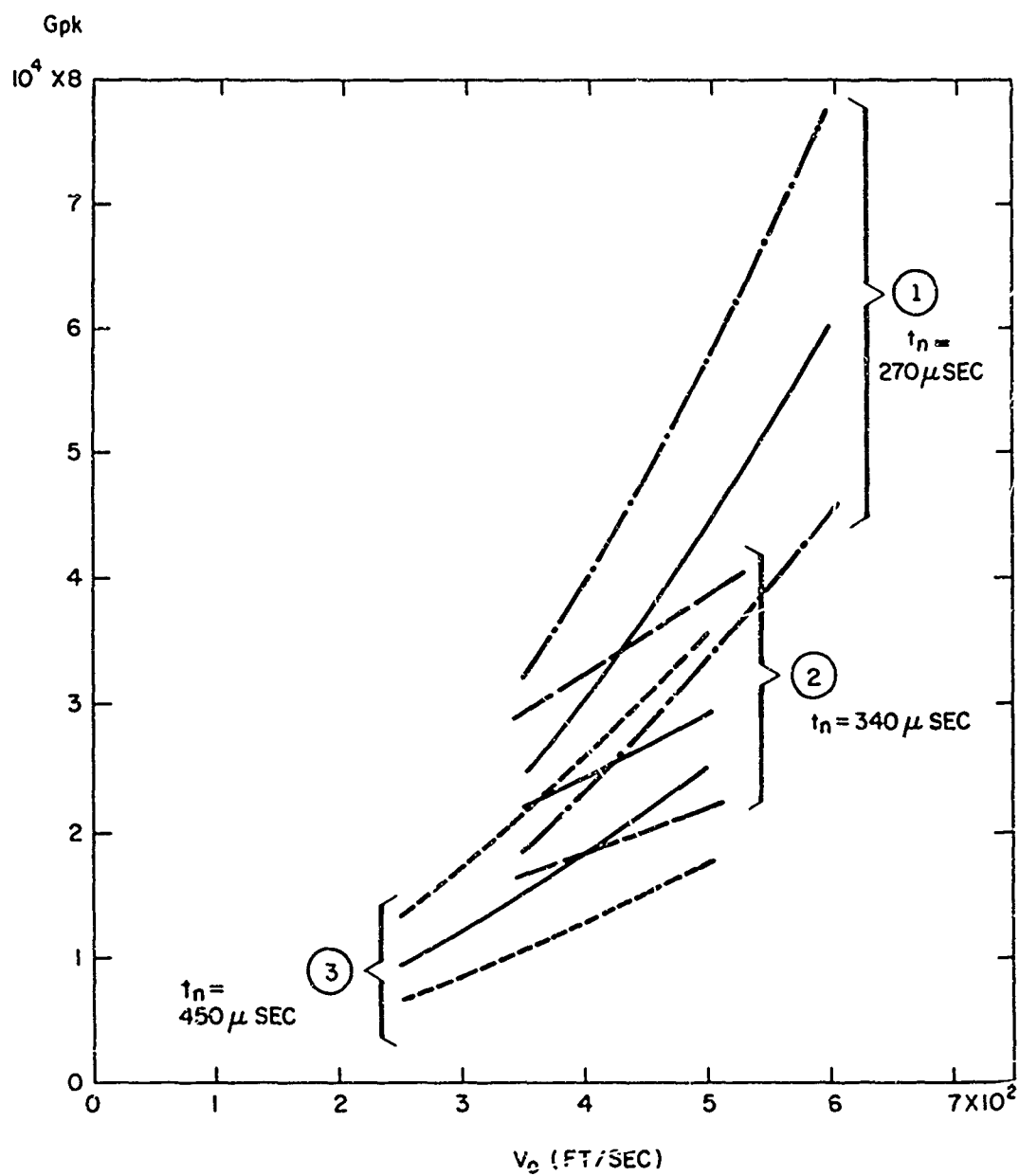
13

Figure 2. Peak g and 95-percent confidence limits measured
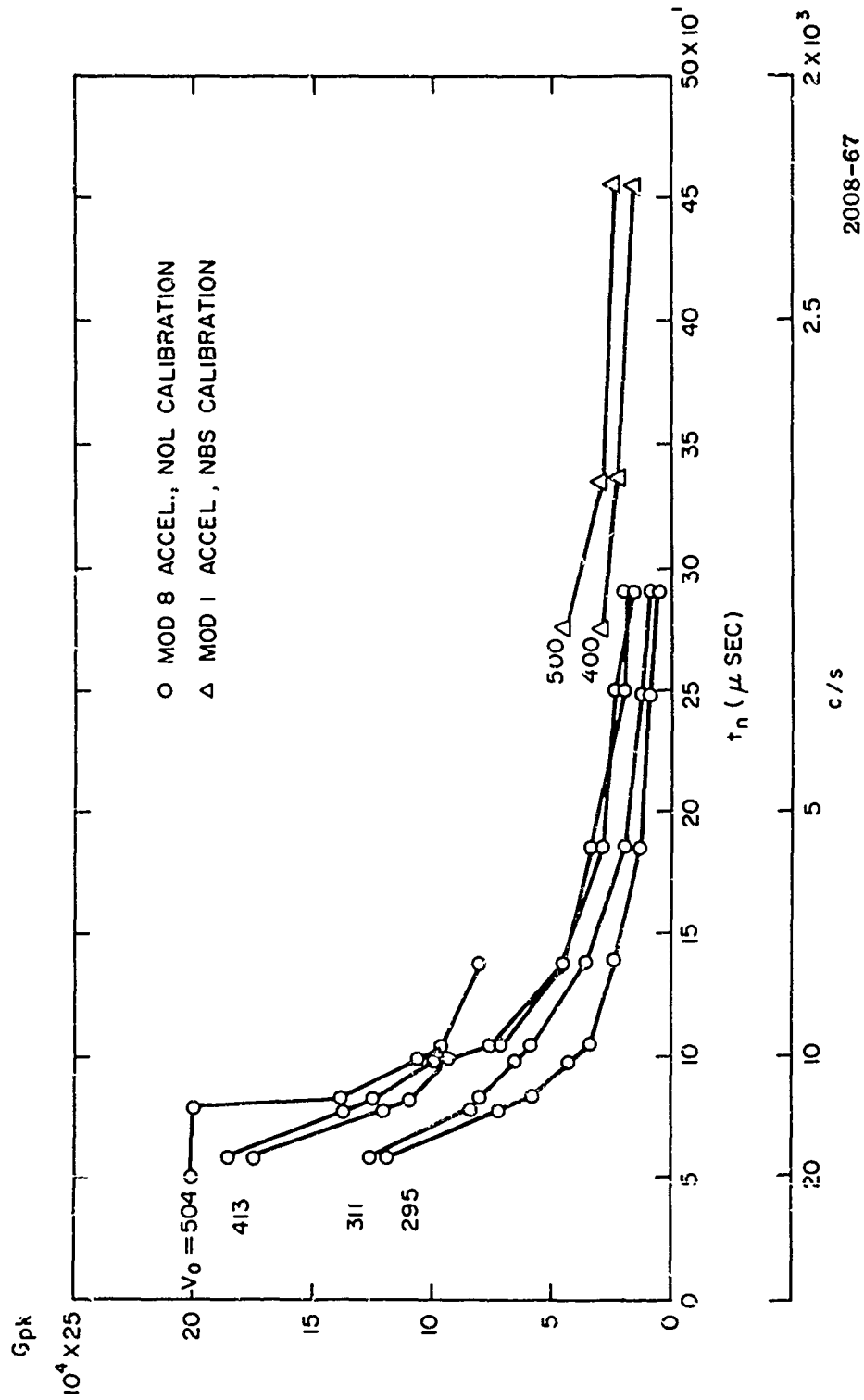at projectile nose versus impact velocity

Figure 3. Peak g for different impact velocities measured at projectile nose versus natural period.

2008-67

The agreement between the two runs made at 413 fps indicates good precision of the measurement. The disagreement between the two types of accelerometers in the overlap region of the 400-fps curves amounts to 10,000 g but lies within the precision indicated by the confidence limits of figure 2. Within these limits the difference in the projectile weights (17.0 lb for the Model 8 data versus a nominal 17.5 lb for the Model 1 fitted data) has no effect. Figure 3 confirms that the forces experienced by the copper ball accelerometer and any component tested in the 4-in. air gun are quite sensitive to the component's natural period. The cause of the large acceleration levels at the short periods is unknown but may be the ringing of the nose and projectile, sharp impulses generated by relative motion between sections of the projectile, or sudden, sharp blows experienced by the projectile in the course of the penetration process or as it rebounds into the catch box walls.

The copper-ball data in the previous discussion were taken from accelerometers mounted on the nose. Runs were made to compare these data with data taken from copper balls mounted in the cargo section. Figure 4 shows the two 413-fps shock spectra that were shown in figure 3, together with a 412-fps shock spectrum obtained from the Model 8 accelerometer mounted in the cargo section. The readings of the nose accelerometer are considerably higher than those of the cargo accelerometer at short natural periods and approach each other at the longer periods.

The response of devices having natural periods longer than those of the Model 8 accelerometer were obtained, using different Model 1 accelerometers (test conditions being the same). The resulting data given in figure 4 show that the response of low-frequency devices mounted in the nose is less than the response of similar devices mounted in the cargo section, the opposite being true for high-frequency devices.

A series of runs was made to investigate the effect of target thickness on G_{pk}. The impact velocity for the 17.0-lb projectile was kept constant at 300 fps. Model 1 accelerometers were used in both the cargo and nose sections. The results are shown in figure 5; two sets of runs were made on different days and are labeled runs A and B in this figure. Although there is variation in the data— the cargo section showing more variation than the nose section— no trend is discernible, which indicates that the target thickness has no effect on the peak-g readings. To check this point further the 17.5-lb projectile's G_{pk} data gathered over a period of years was fitted by means of a straight line to the target thickness.
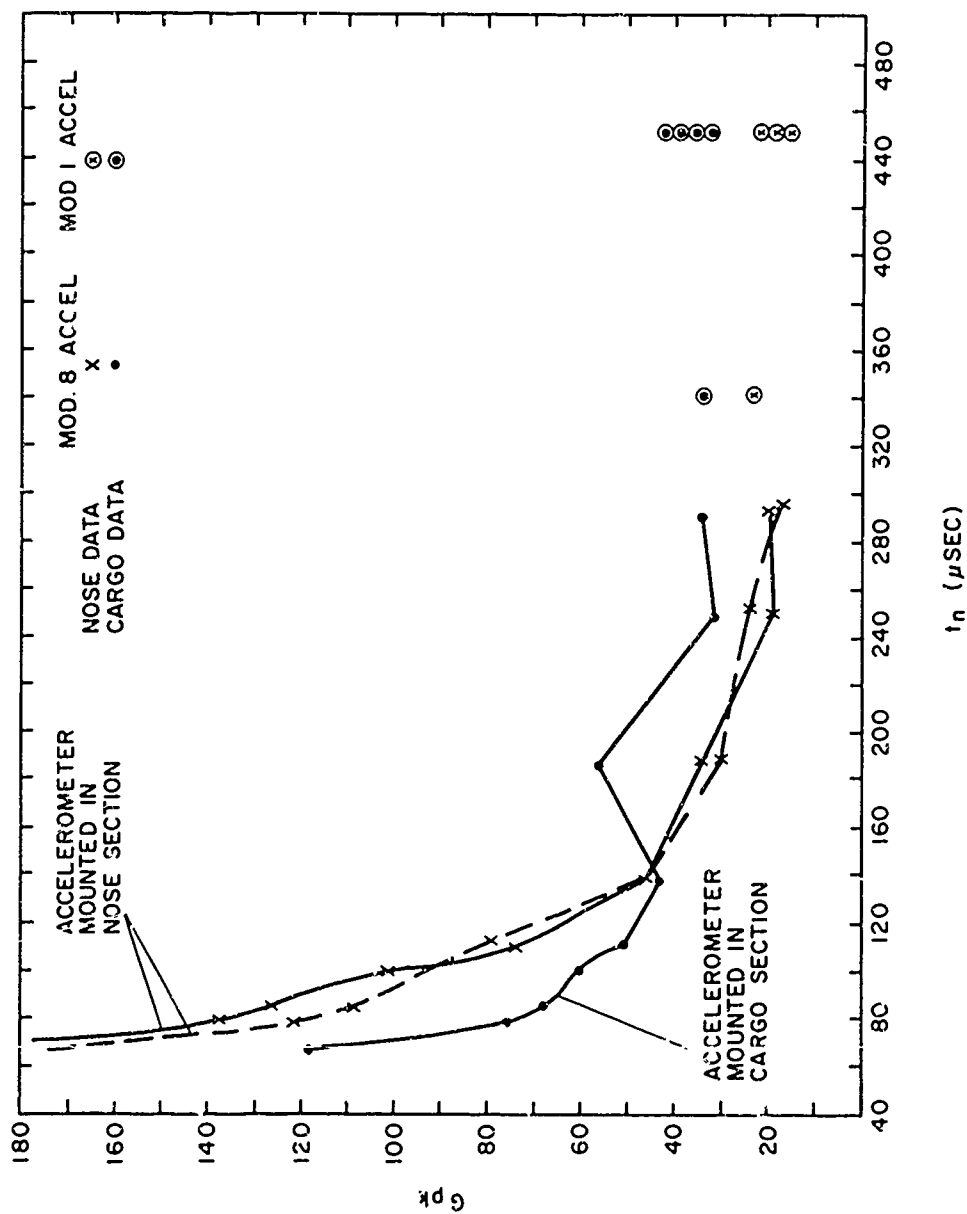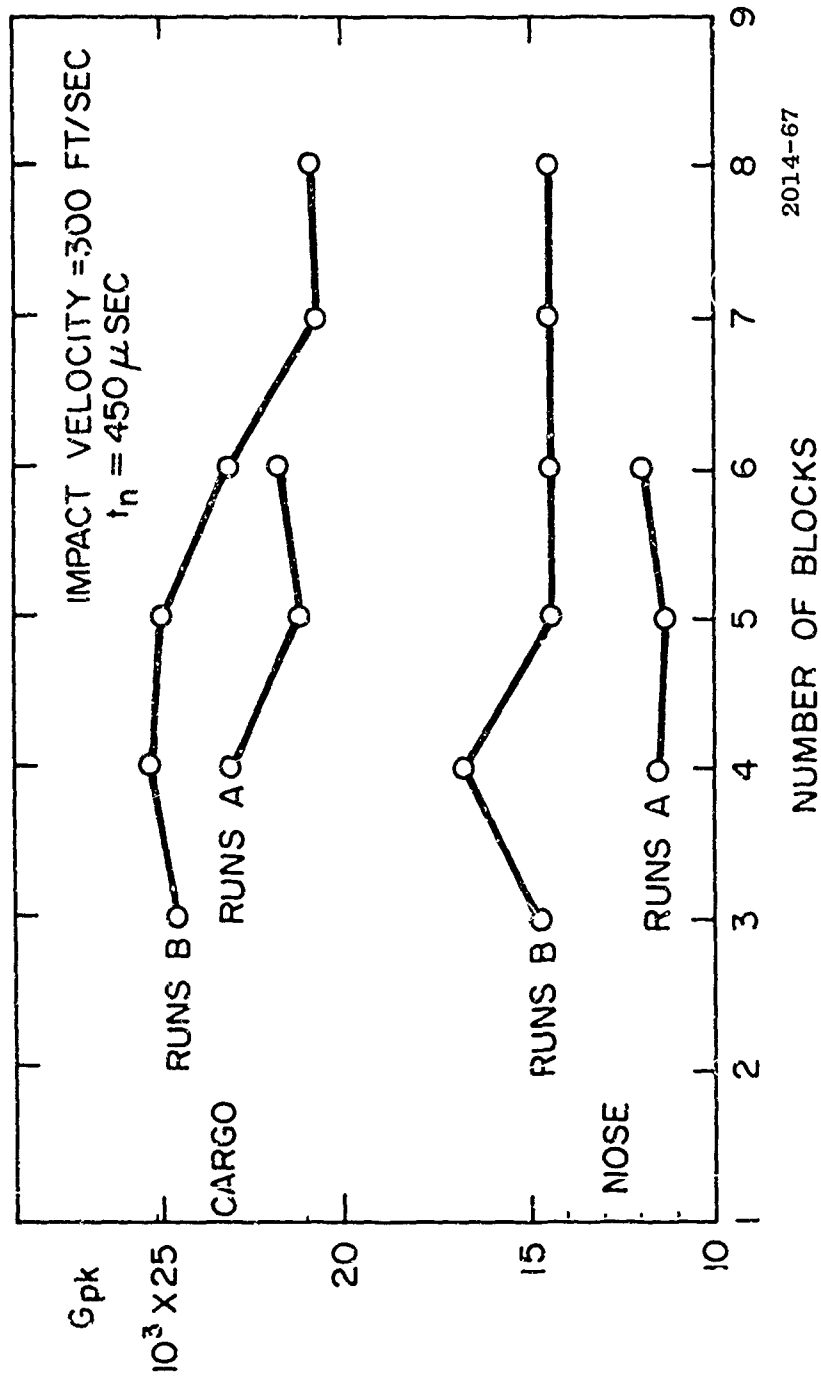
Figure 4. Peak g measured at nose and at cargo sections as a function of natural period of accelerometer.

17

Figure 5. Peak g measured at the projectile nose and cargo sections as a function of the number of lead target blocks.

18

The correlation function of this fit was 0.761, indicating a dependence between G_{pk} and target thickness. The reason for this inconsistency as well as the reason for the change in levels (runs A and B of figure 5) is unknown.

The dependence of the copper-ball accelerometer reading on the depth of penetration is given by the data fit described in appendix A. As plotted in figure 6, the low-frequency data for both 17.5- and 23.0-lb projectiles follow the same trend. The high-frequency response is completely different.

The dependence of G_{pk} on the mass of the projectile can be seen by examining the G_{pk} - v_o fit (apx A) for 17.5- and 23.0-lb projectiles. A statistical t test of the exponents of the projectile's $t_n = 340$-μsec data indicates that, within a 95 percent confidence limit, these exponents actually differ from one another.

4. SUMMARY AND CONCLUSIONS

The primary measuring instrument used in this evaluation study was the copper ball accelerometer. The data generated by this device must be questioned when used in an undefined situation such as existed in air-gun impact tests.

The copper ball accelerometer with high natural frequency has indicated peak accelerations up to 200,000 g (fig. 3). It is unlikely that the peak retarding force offered by the target material has this magnitude. The accelerometer measurements still yield valid information, however, if they are interpreted as a shock spectrum—that is, as the response of structural members. The deformation of the copper ball in the high-frequency accelerometers may be due to a pulse of extremely high amplitude and short duration, or the deformation may be caused by the cumulative effect of a number of low-amplitude impulses. Whichever case it may be, the response is a complicated one and the use of the air gun as an impact test for high-frequency components is questionable. The center of mass of the projectile and its cargo follow the trajectory demanded by the retarding force of the target. The fact that there is a difference in the copper-ball-accelerometer readings in the nose and in the cargo section, therefore, shows that the structure of the projectile is contributing significantly to the pulse experienced by the test specimen.

Various theories were applied to the lead-target penetration process and the measured penetration depth and impact velocity are compared with the theoretical expressions in appendix B. None of the theories used are known to have been applied to the penetration
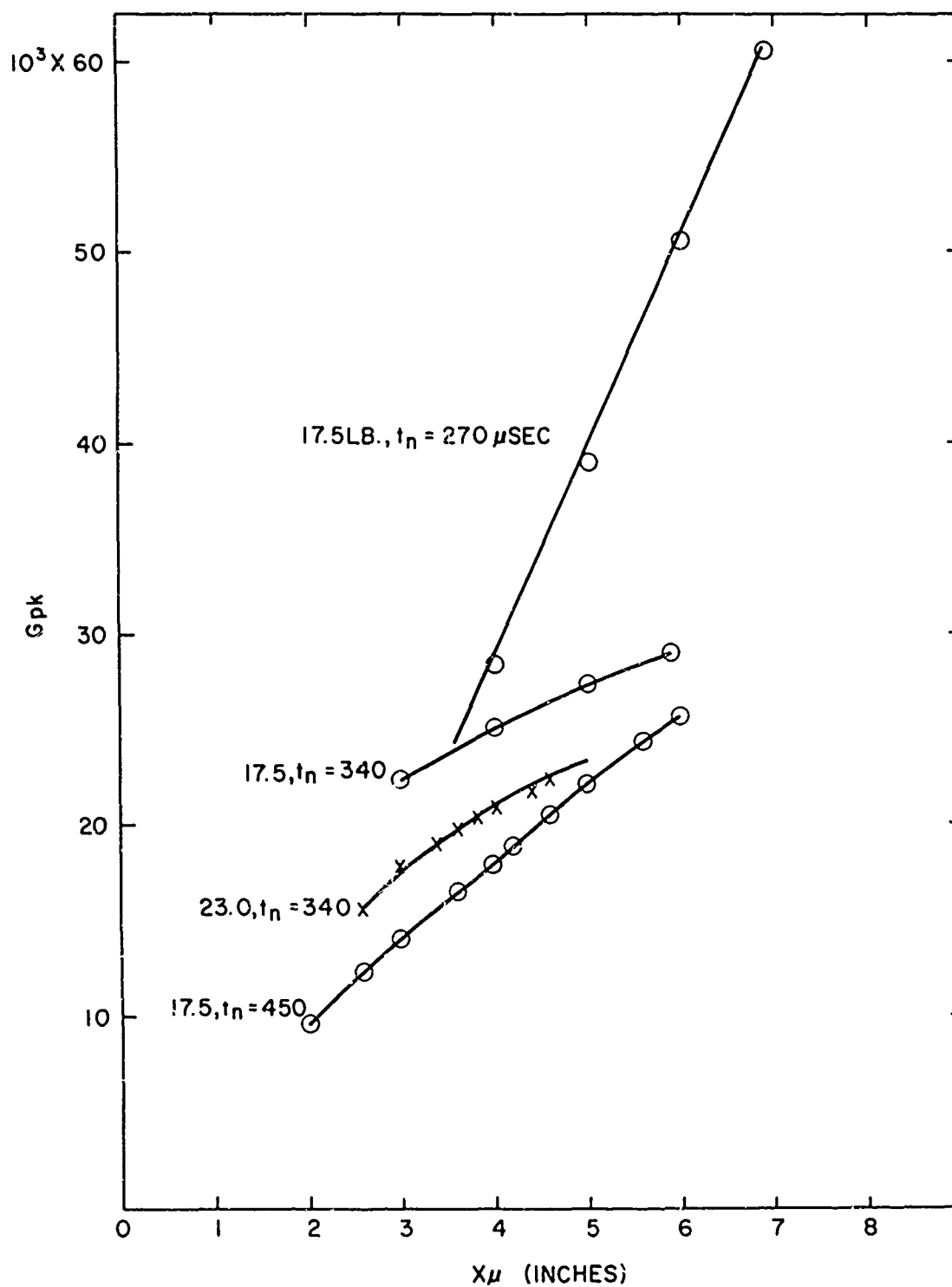
Figure 6. Peak g measured at projectile nose versus depth of penetration.

of lead in the velocity range under study and their validit· is un-
known. Despite this uncertainty, study of the data and various
comparisons allows the following conclusions.

(a) A constant pressure model evaluated with the assumption
of shallow penetration depth predicts a penetration time inde-
pendent of impact velocity. Without the shallow depth approximation,
this model would predict a penetration time that would vary with
impact velocity. Although a closed form solution to this model was
not obtained, it deserves further attention, particularly in the
case of low-velocity impacts.

(b) The Poncelet equation, widely used to predict penetration
depths, assumes that the peak force is reached at the instant the
projectile contacts the target. This is of questionable value here
since projectiles with ogive shaped noses show a rise time (ref 3,
p 306).

(c) The crude assumption of a constant force is widely used
to get estimates of peak forces in impact testing. In the study
made here, this law predicts penetration times that are in fair
agreement with the measured penetration times (fig. 7). The pene-
tration time, however, is an insensitive discriminator between the
force laws described herein. The peak g's calculated assuming this
law (fig. 8) agree approximately with the peak g's measured with
low-frequency accelerometers (fig. 3) provided that the measured
values are divided by 2, as they would be if the applied force were
a square pulse (ref 2). Thus, the peak g calculated for a 400-fps
shot would be 7100 g, whereas the averaged Model I accelerometer
data from figure 3 is 18,300 g or 9150 g if the dynamic character
of a square wave applied force is considered.

It is concluded that, although the test is a convenient and
an inexpensive means of subjecting fuzes to high-force levels, un-
controlled test variations and the high-frequency response of the
projectile make a cautious approach to quantitative interpretation
of the results necessary.
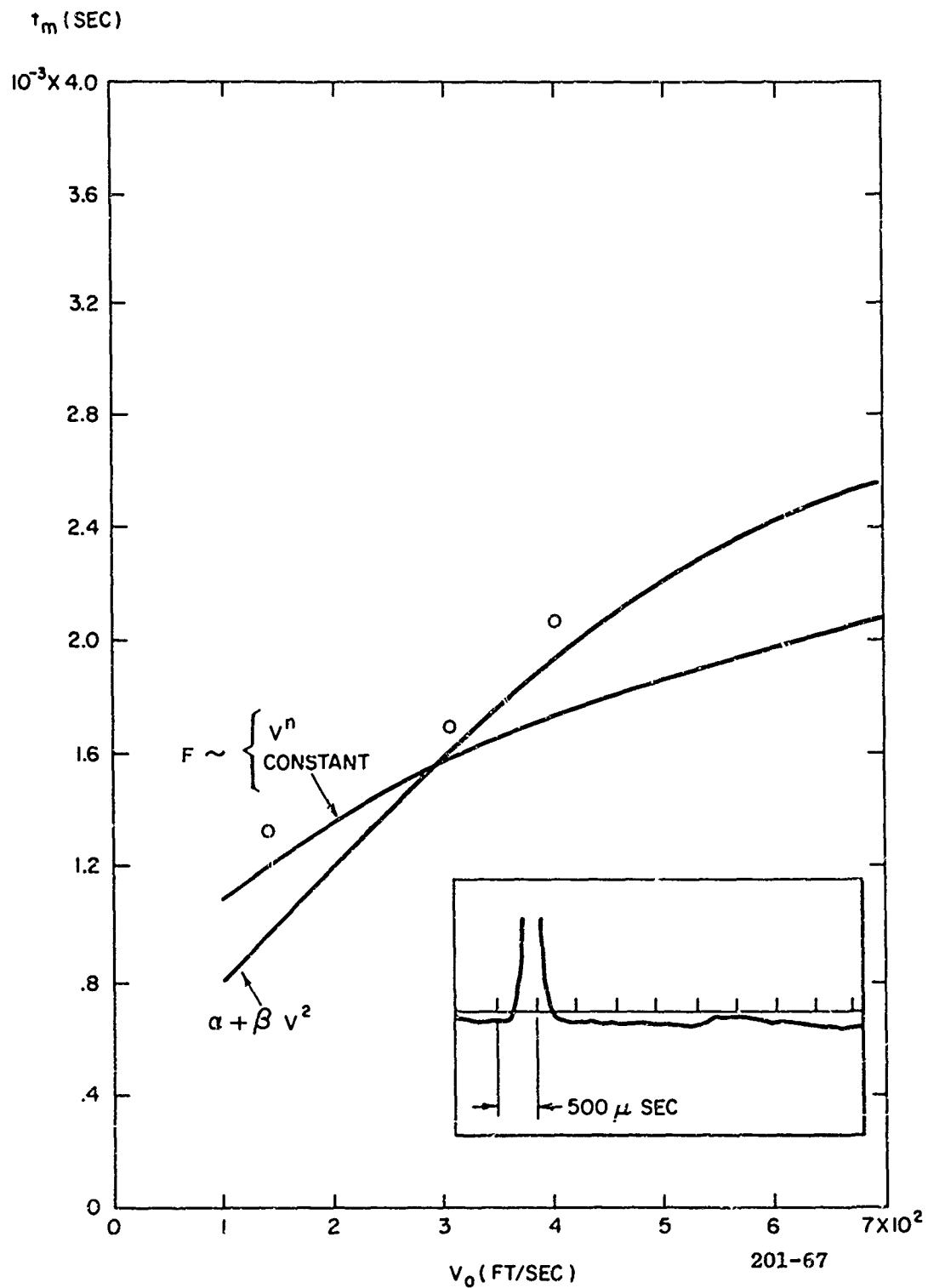
ACKNOWLEDGEMENTS

Figure 7. Penetration times calculated for various penetration models together with measurements.
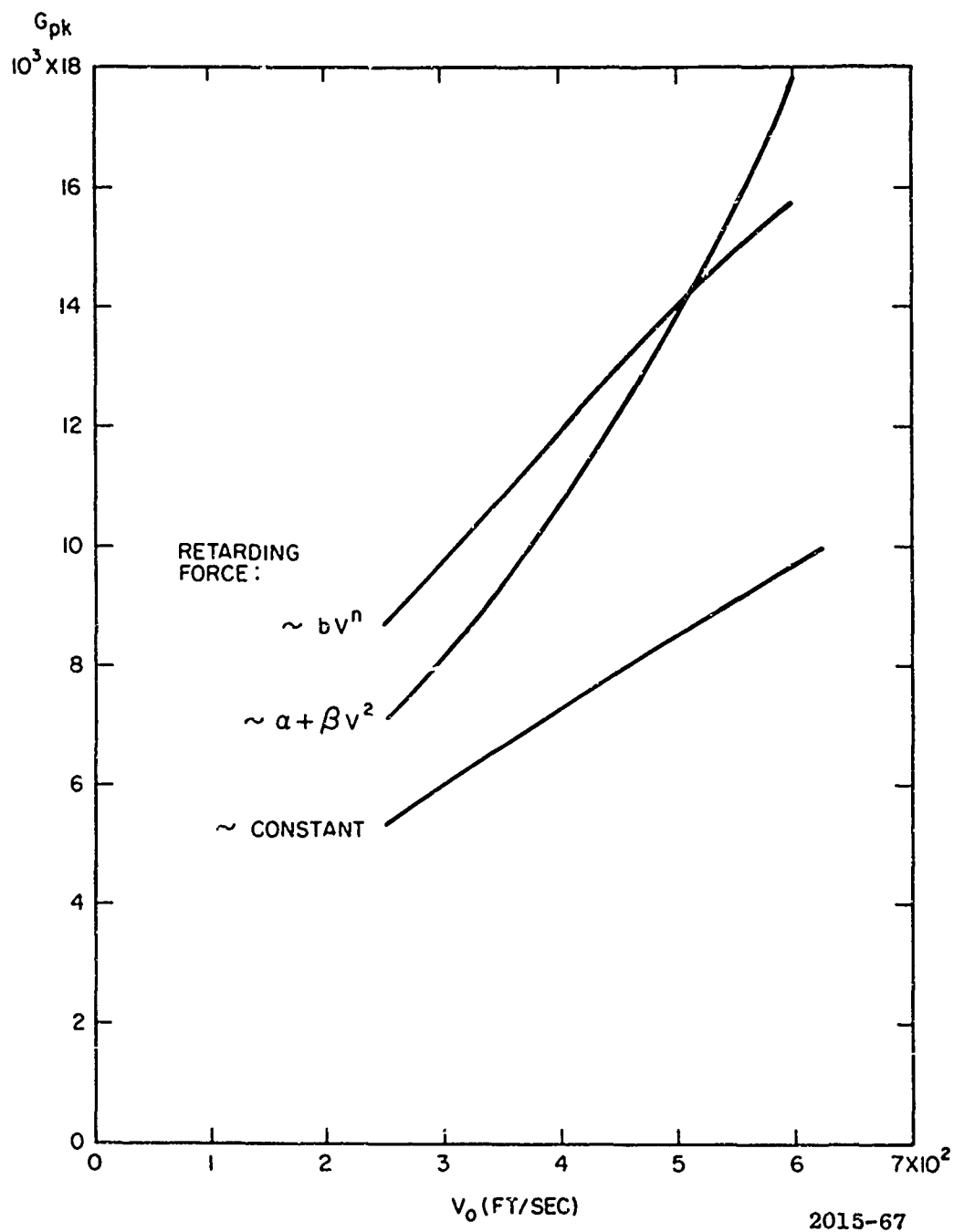
Figure 8. Peak g calculated for various force equations.

APPENDIX A. FIT OF EXPERIMENTAL DATA

The data accumulated in 4-in. air-gun tests over a three-year period were punched on cards and computer fitted by a least squares technique to curves of the form

$$X = c \, Y^p$$

where c and p were determined by the fit and suitable pairs of quantities listed in table I were substituted for X and Y. The actual fit was made to the straight line formed by taking the logarithm of the above expression.

The results are shown in tables II (a) and II (b). The number of points used in each fit together with the velocity range covered by the data are also given. The results of the fit for projectiles weighing 17.5 and 23.0 lb are shown together with the results for 17.5-lb projectiles which penetrated less than 2 in.—that is, less than the radius of the projectile nose. The standard 17.5-lb. projectile data are subdivided into three parts in table II (a) since three different copper ball accelerometers were used, each with its own natural period as shown in the table. σ_p is the standard deviation of the exponent p.

The peak acceleration is in multiples of g, the velocity in fps, the pressure in psi and the penetration depth is in in.

Preceding Page Blank

APPENDIX B.   PENETRATION PHENOMENA

The retarding force experienced by the projectile is determined
by the phenomena encountered while penetrating the lead target.
Since there were no dynamic force measurements, the available data
were used to gain some insight into these phenomena. The 734 ex-
perimentally determined penetration depths listed in table II (a)
for the 17.5-lb projectiles were fitted to the impact velocity,
yielding

$$x_m = 1.167 \times 10^{-4} \, v_o^{1.33},$$

where x_m is in feet and v_o is in feet per second. The residual of
this fit is -0.7078, the standard deviation of the residual being
2.76×10^{-7}.

The value of 1.33 for the exponent of v_o has been noted in
other investigations (ref 4) as characteristic of relatively low-
velocity penetrations. In ballistic work it is known as the De Marre
law of penetration. The observation has also been made (ref 4) that
the exponent tends toward values less than 1.33 with increasing
impact velocity. The data fitted here show this trend, as can be
seen in table II (a). The fact that there is a velocity dependence
argues against the hydrodynamic analysis used in high-velocity
impacts, such an analysis predicting a penetration depth which is
independent of impact velocity (ref 4).

The x_m - v_o fit to 17.5-lb shallow penetration data yields an
exponent of 1.267 (table II b). This low value occurs despite the
fact that the data were taken over a range of low velocities. This
value indicates that different phenomena govern the penetration
behavior in the shallow and deep penetration regimes. Similar be-
havior has been noted in other materials (ref 5). The value of the
fitted exponent argues against using the shallow penetration Hertz
law (ref 3) over the velocity range in question since this law
predicts that the impact velocity is raised to the 0.8 power.

The number of lead blocks used in each run is varied in the
interests of economy. The minimum thickness of unpenetrated target
material is usually more than 1/2 in. The penetration-depth/target-
thickness data for the 17.5-lb projectiles already discussed were
fitted to a straight line. The resulting correlation coefficient
for this fit was 0.86, indicating that the penetration depth is
dependent upon the target thickness. To check this statistical
evidence experimentally, runs were made with a 17.0-lb projectile,
impact velocity being 300 fps. No trend could be detected in the
data within the accuracy of the depth measurement.

26

The existence of a crater-depth/mass-of-projectile dependence can be seen by examining the x_m - v_o data fit (table II) for 17.5- and 23.0-lb projectiles. A statistical t test of the exponents of the projectiles t_n = 340 µsec data indicates that, within a 95-percent confidence limit, these exponents actually differ from one another.

Visual inspection of the craters indicates that the spherical nose of the projectile always matches the contour of the crater in the vicinity of the nose. The surface of this part of the crater is smooth and bright and has a different appearance from that of the after part of the crater. The crater diameter at the surface of entry is greater than the diameter of the projectile, the diameter at the entrance of a 6-1/2 in. deep crater being 4-3/8 in. These effects can be seen in figure 9. Table III* gives data pertinent to figure 9.

The jagged lip around the edge of the crater (as typified by those of figure 7) and small particles of lead on the catch box floor indicate that the lead flows or melts during the penetration process. The surface of the crater appears to be a very thin layer of lead, which may be picked off in strips. This can also be seen in figure 9.

It was noted after a series of shots that there was a flattening of the projectile nose. As the flattening for a single run was very slight this effect was ignored.

These observations show that the kinetic energy of the projectile is being dissipated in several ways including the plastic deformation of the target and projectile material, the melting of the target material, and the transmission of energy to far parts of the target system by various types of waves. Although it is reasonable to assume that the predominant dissipative mechanism varies with the kinetic energy of the projectile, an attempt was made to find a single force law describing the penetration of the projectile over the entire velocity range.

One approximate assumption used was that the velocity of the projectile decays linearly as it progresses through the target, the retarding force being contant. Integrating the equation of motion, using x = o and $\dot{x}$ = v_o when t = o and applying the necessary condition that $\dot{x}$ - o when the penetration process is over, yields

$$x_M = \frac{v_o^2}{2a} \qquad \text{(B-1)}$$

and

$$t_M = \frac{v_o}{a} \qquad \text{(B-2)}$$
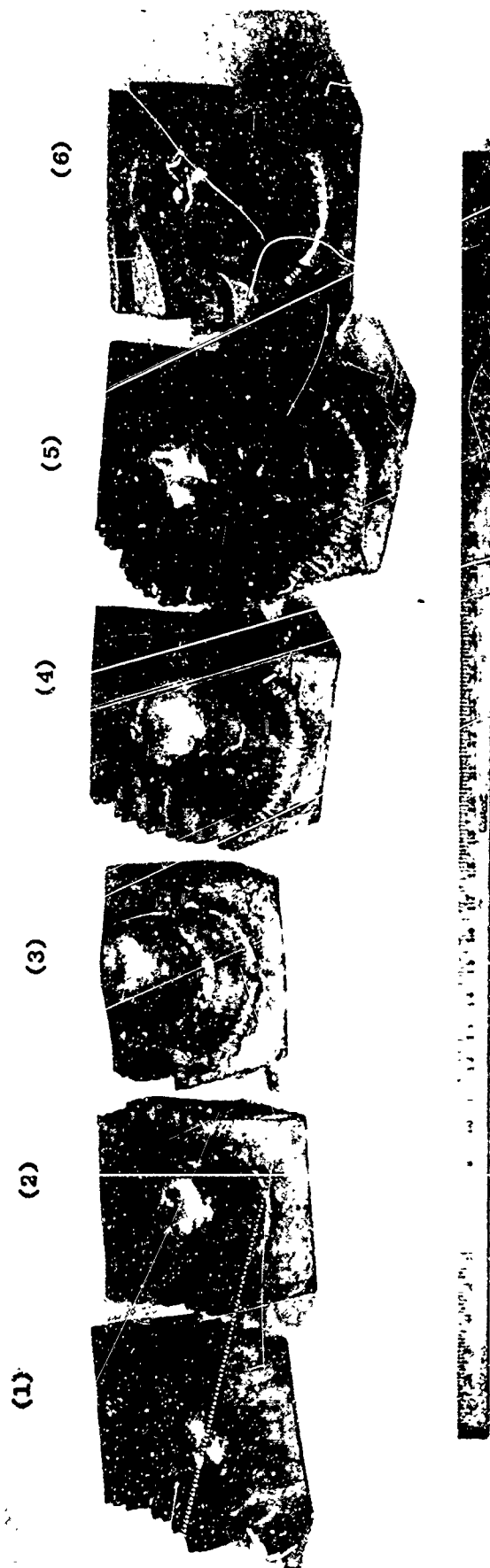
---

*See page 34

(1) (2) (3) (4) (5) (6)

1845-66

Figure 9. Target craters resulting from different velocity impacts. (See table III.)

The Poncelet equation has been used to express penetration processes of ordnance material since the early 19th century (ref 5). In its classic form this equation of motion can be expressed as

$$-m \frac{d^2 x}{dt^2} = \alpha + \beta v^2,$$ (B-3)

where α and β are constants.

Integrating and using the same initial conditions as above yields

$$x_M = -\frac{m}{2\beta} \ln(1 + \frac{\beta}{\alpha} v_o^2),$$ (B-4)

$$t_M = \frac{m}{(\alpha b)^{\frac{1}{2}}} \tan^{-1}(\sqrt{\frac{\beta}{\alpha}} v_o),$$ (B-5)

and

$$(\frac{dv}{dt})_{peak} = -\frac{1}{m}(\alpha + \beta v_o^2).$$ (B-6)

Another force law assumes that the force acting on the projectile depends on the instantaneous velocity raised to a power. This yields as the equation of motion

$$m \frac{d^2 x}{dt^2} = -b \, v^n,$$ (B-7)

with the result after integration

$$x_M = \frac{m}{(2-n)b} v_o^{(2-n)},$$ (B-8)

$$t_M = \frac{m}{(1-n)b} v_o^{(1-n)},$$ (B-9)

and

$$(\frac{dv}{dt})_{peak} = -b \, v_o^n.$$ (B-10)

This law is discussed for the sake of completeness, simple velocity dependent laws being primarily applicable to the cases of gases and granular solids (ref 5).

Using the x_M obtained from the v_o fit for the 17.5-lb projectile given in this appendix, the acceleration for the constant force law was evaluated using equation B-1 after the constants for the velocity-dependent force law were obtained by equating this fit to equation B-8. The Poncelet predicted depths were fitted from the original 17.5-lb projectile data to the expression

$$x_M = k_1 \, \ln(1 + k_2 \, v_o^2)$$

where x_M was in ft and v_o was fps. The results are

$$k_1 = 0.431 \text{ ft}$$

$$k_2 = 7.4 \times 10^{-6} \left(\frac{ft}{sec}\right)^{-2}$$

The conversion of k_1 and k_2 to α and β was done using equation B-4. The constants resulting from these fits are shown in table IV.[*] The peak forces calculated from equations B-1, B-6, and B-10 are shown in figure 8. The peak g predicted by the constant force law is less than that predicted by the other laws. When comparing these results with the copper ball accelerometer measurements, note that the response of the ball to a dynamically applied force is not the same us that to a static force such as was used in the calibration of the ball (apx D). Thus, the true force seen by the low-frequency accelerometer would be half that actually indicated if the constant force model were the correct one.

Recent work in the Soviet Union (ref 6) yields:

$$x_M \simeq \frac{\ell}{2k_o} \cdot \frac{\rho_p}{\rho_T} \ln\left(1 + \frac{k_o \rho_T}{H_T} v_o^2\right).$$

This is the same form as the integrated Poncelet equation. Using the material constants given in reference (6) for the 17.5-lb projectile, we find

$$-\frac{\ell}{2k_o} \frac{\rho_p}{\rho_T} = 9.37 \times 10^{-2} \text{ ft}$$

$$\frac{k_o \rho_T}{H_T} = 2.18 \times 10^{-6} \left(\frac{ft}{sec}\right)^{-2}$$

---

[*]See page 34

30

While the agreement between the fitted and calculated results is far from exact, this comparison indicates that the constants of equation B-7 can be used for estimation purposes when predicting penetration depths.

Another theory used to describe low-velocity penetration processes assumes that the target material exerts a constant "dynamic flow pressure" p on the projectile as the penetration process takes place. Although a highly speculative assumption, it yields interesting results. The equation of motion for a round-nosed projectile becomes

$$m \frac{d^2x}{dt^2} = -p\pi(Dx - x^2)$$

$$\approx -p\pi Dx.$$

The last step is an approximation valid when $x \leq D/2$. Integrating this equation, we obtain

$$x_M = v_o \left(\frac{M}{\pi Dp}\right)^{\frac{1}{2}}, \tag{B-12}$$

$$t_M = \frac{1}{2} \left(\frac{\pi m}{Dp}\right)^{\frac{1}{2}}, \tag{B-13}$$

and

$$\left(\frac{dv}{dt}\right)_{pk} = v_o \left(\frac{\pi Dp}{m}\right)^{\frac{1}{2}} \tag{B-14}$$

Table II (b) gives data for 68 points where $x_M \leq D/2$. The average pressure obtained from these data using equation B-12 was 13,000 psi. This compares favorably with the 12,000-psi figure given in reference 6, page 96. It also agrees with the 13,000 psi obtained by McCarty (ref 7) who fitted peak acceleration-impact velocity data. However, McCarty's fit of penetration depth-impact velocity data yielded 21,000 psi. The constant pressure theory as developed here predicts a penetration time independent of impact velocity. This time is 0.82 msec for the 17.5-lb projectile if p = 13,000 psi.

A measurement of the penetration time was made by placing a commercial strain gage on a steel block behind the lead target blocks. No attempt was made to interpret the strain amplitude obtained, but the duration is believed to be close to the projectile deceleration time. One of the traces is sketched as the insert of

31

figure 7. Three data points were obtained by this means and are shown in figure 7 together with the durations predicted by constant-force, velocity-dependent, and Poncelet force laws. The times predicted by the first two laws are identical, the penetration times predicted by all three laws being quite similar. The fact that there is a variation in penetration time rules against the constant pressure law as presented here.

Cutting open various target blocks showed that the projectile was moving away from the steel table as it moved through the target. In addition, the tops of the blocks were splayed apart while the bottoms had a compressed appearance. The climbing angle was measured by taking the horizontal distance to the end of the crater and the vertical distance from the center at the entrance of the crater to the center of the crater at its end. These angles are listed in table III.

The effect of the climbing angle on the final target penetration depth is believed to be small and was ignored in the analysis made here. An estimate of the transverse forces acting on the projectile was made using an expression based on a constant force model

$$a = \frac{8y}{t^2_M}$$

where y is the measured transverse displacement of the projectile and t_M is the corresponding constant force time duration taken from figure 8. This results in an estimate of 16,000 to 20,000 peak g's acting transversely on the projectile in the velocity range of 400 to 500 fps.

Assuming that the climbing of the projectile and that the no symmetrical deformation of the target were due to wave phenomena, the target blocks were placed on rails so that only a small portion of the target's bottom surface was in contact with the steel surface of the support table. The climbing and non-symmetry were eliminated. Figure 7, blocks (5) and (6), are targets used with and without rails.
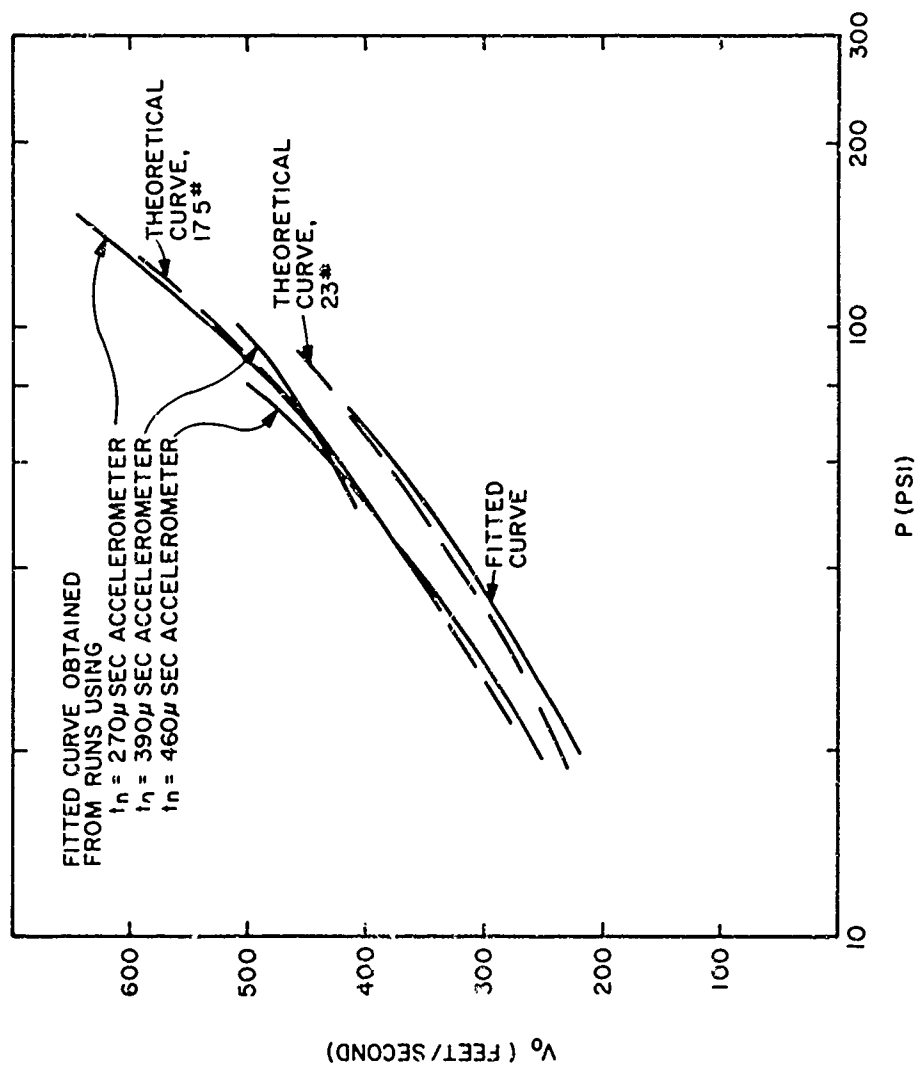
Figure 10. Experimental and calculated muzzle velocities as a function of gas driving pressure for projectiles of different weight.

Table III. Characteristics of Target Blocks

Figure 6 target No.	v_0 (fps)	x_m (in.)	Number of lead blocks used	Diameter at entrance to crater (in.)	Angle of climb (deg)
1	223	1-1/2	6	3-7/8	0
2	390	4	6	4-1/2	5-1/2
3	521	4-3/4	7	4-7/8	-
4	520	5-1/2	6	4-7/8	6-1/2
5	538	6	10	5-3/8	11-1/5
6	558	5-1/8	7	-	0

Table IV. Results of Fitting Force Laws

(v in fps)

$F = b\ v^n$	$F = \alpha + \beta\ v^2$
b = 293.9	$\alpha = 3.52 \times 10^4$
n = 0.770	$\beta = 0.628$

34

APPENDIX C. DRIVING PRESSURE-VELOCITY BEHAVIOR OF PROJECTILE

The dependence of the shell velocity upon the pressure of the driving gas is important in the design and operation of air guns. If it is assumed that the air gun has an infinite length pressure chamber and is of constant diameter overall, that the driver gas is thermodynamically ideal, and that there are no energy losses in the system, the dependence of the projectile muzzle velocity upon the initial pressure of the driving gas may be shown to be (ref 8)

$$P_o = \frac{a_o^2 m}{A\,L}\left(\frac{2}{\gamma+1}\right)\left[1 - \frac{1-\left(\frac{\gamma+1}{2}\right)U_o}{(1-\frac{\gamma-1}{2}U_o)^{\frac{\gamma+1}{\gamma-1}}}\right].$$

Figure 10 plots this relation for 17.5- and 23.0-lb projectiles assuming $\gamma = 1.4$ and an initial gas temperature of 300°K. A comparison is made to relations fitted to the experimental data (apx A). The 17.5-lb projectile curves shown in figure 10 correspond to data obtained while using three different accelerometers, but are independent of which accelerometer was used. The agreement is considered good in view of the assumptions made in the theory.

The driving force acting on the shell is equal to gas pressure times the area of the shell. On this basis the accelerations experienced by the projectiles fired from the 4-in. air gun range from 20 to 100 g depending upon their weight and muzzle velocity. These accelerations are considerably less than the decelerations experienced upon impact.

APPENDIX D. CHARACTERISTIC OF COPPER BALL ACCELEROMETERS

Copper crusher gages have been in use since the nineteenth century, intensive development taking place during and after the World Wars. Gages have been designed to measure pressures generated in underwater explosions (ref 9-12) and the pressures generated in artillery weapon firings (ref 13). The U. S. Navy has made considerable use of copper crusher accelerometers. The series of accelerometers developed by the U. S. Naval Ordnance Laboratories (ref 2) have found wide acceptance. Accelerometers are often used to determine the forces acting on a system.

Figure 11 is a schematic of the essentials of one of these gages. The proof mass is designed so that it may be varied. The radius of the surface in contact with the copper ball is nominally 1-1/2 in. The crushed element is an annealed copper ball, 5/32 in. in diameter. A rubber sleeve is used to hold the ball to the anvil, which is rigidly fixed to the projectile. In simple models, a small screw is made finger tight behind the proof mass to prevent the system from rattling in the cylinder. Variations of this basic design and different techniques of using the gage are described in reference 2. Conceptually, it is taken to be a spring-mass system, the analogy to the actual gage being shown in figure 7.

The plastic deformation taking place when the mass crushes the copper ball is assumed to be linear with the applied force. The slope of a static calibration curve then yields the spring constant, k. This, together with the proof mass, defines the natural frequency of the gage, namely:

$$f_n = \frac{1}{2\pi} \sqrt{\frac{k}{m}} .$$

To obtain the peak forces acting on the system, the deformation of the ball is obtained by measuring the diameter of the ball before and after a run. Then using the expressions

$$F_{Dynamic} = m'a_{Dynamic} \approx \frac{w'}{g} a_{Dynamic} = k X_{Dynamic},$$

we obtain

$$G_{Peak} = \frac{a_{Dynamic}}{g} = \frac{k}{w'} X_{Dynamic},$$

where w' = weight of proof mass,

and

m' = proof mass.

RESTRAINING
CYLINDER

RUBBER
RESTRAINING
SLEEVE

MASS

COPPER BALL-
SPRING

2011-67
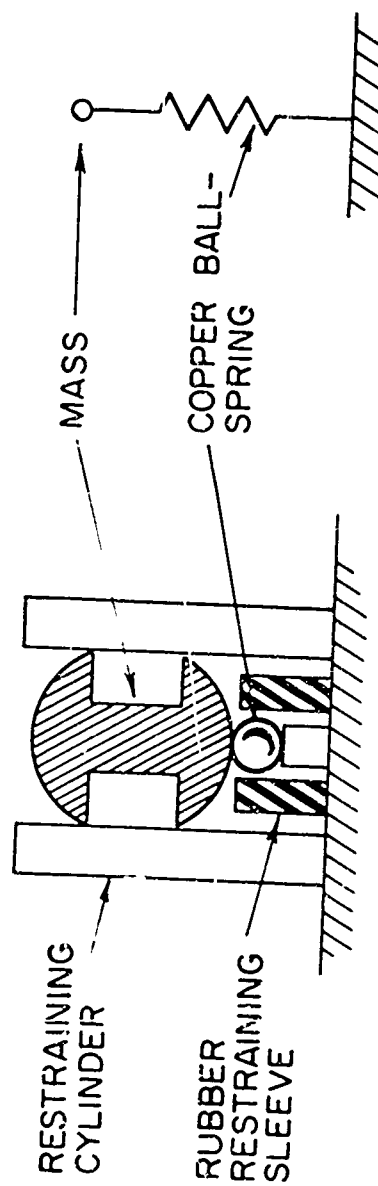
Figure 11. Model of copper ball accelerometer and spring-mass
analogy.

Subscripts refer to static or dynamic use of the gage.

Note that

$$\frac{k}{w'} X_{Dynamic} = \frac{F_{Static}}{w'} \frac{X_{Dynamic}}{X_{Static}}$$

and, therefore, the measured G_{peak} is proportional to the normalized displacement response usually obtained from a shock spectrum analysis (ref 14).

The copper ball accelerometer has the advantages that it is rugged and capable of measuring peak forces in the range of hundred of thousands of g's. It is a highly reliable instrument in the sense that it seldom fails to operate. In addition, it is relatively inexpensive to build and use. It is self-contained and thus requires no external signal leads, modifiers, etc.

One of the disadvantages of copper ball accelerometers is that the static force-deformation curve is nonlinear, as can be seen from figure 12. Four calibration curves of four different batches of 5/32 in. diameter balls are shown—one calibration from Harry Diamond Laboratories (HDL); one from the National Bureau of Standards (NBS); two from the Naval Ordnance Laboratory (NOL), NOL curve (1) from reference 2 and NOL curve (2) from the slowest applied force curve in reference 15. The use of straight lines drawn through these curves decreases the accuracy of an amplitude measurement, but the resulting error is slight if the deformation of the ball is kept small. The slope of the curve may be obtained from a straight line drawn through the nonlinear calibration curve or by taking the slope at a specified point on the curve.

The major problem that occurs when using a static calibration curve is the discrepancy between dynamically and statically caused deformations. The shock spectra (ref 10-12, 14) for a one-dimensional spring mass system show that these two quantities are approximately the same when the gage's natural period is greater than the duration of the input pulse for most simple input pulses. This is not true when the natural period is approximately equal to or less than the input pulse, for certain simple input pulses, or when the input pulse is complex. A copper ball accelerometer measurement can be accepted as accurate or correction factors can be applied when there is knowledge or an estimate of the input pulse history.
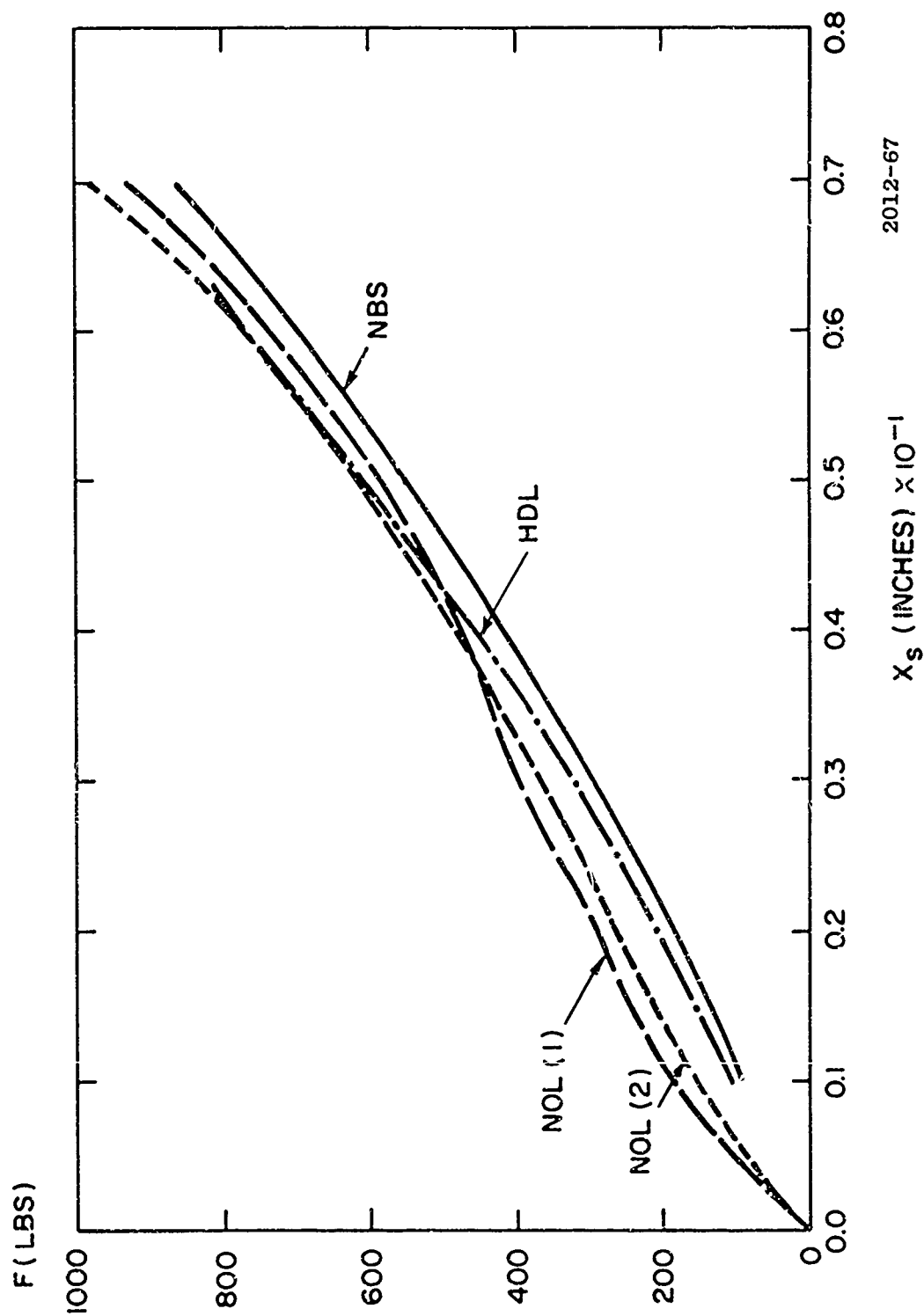
38

Figure 12. Copper ball static calibration curves, ball diameter 5/32 in.

2012-67

X_s (INCHES) $\times 10^{-1}$

F (LBS)

NBS

HDL

NOL (1)

NOL (2)

39

Dynamic studies of copper balls have been made at the Naval
Ordnance Laboratories (ref 15, 16) and additional work is planned.
The discrepancy between copper ball and piezoelectric pressure gage
measurements (ref 17) has been reduced by the dynamic calibration
techniques of Aberdeen Proving Ground (ref 13, 18) using hydrauli-
cally applied half-cycle sine-wave input pulses.

Multiple impacts acting upon a copper ball accelerometer will
cumulatively deform the copper. In shock-type work, the high ampli-
tude peaks caused by the driving force are often accompanied by
higher frequency waves caused by the oscillations of the test vehicle.
The deformation of a ball in a low-frequency accelerometer due to
the high-frequency pulses will be slight but higher frequency acceler-
ometers can be considerably in error, particularly if the duration
of the pulses is comparable to the natural period of the acceler-
ometer. A particular portion of an input pulse can be examined by
using a restraint which falls into place during the application of
the force. The design of such devices is discussed in reference 2.

The test-vehicle structure introduces another source of error
into the analysis of copper ball data. The analysis assumes the
gage is a one-degree-of-freedom system—that is, the deformation of
the ball can be described by one coordinate. A multi-degree-of-
freedom system will result if the gage is mounted on a part of the
structure that moves with respect to other parts. Reference 19
describes the response of a two-degree-of-freedom system to some
simple input pulses and sets up criteria for acceptable data from
such systems.

The characteristics of a copper ball accelerometer which are
described above are listed in table V. The advantages of the gage
are such that its use is recommended in situations where the peak
forces or other environmental conditions are extreme or where there
are cost considerations.

The many disadvantages of the gage can be partially overcome
when it is used in new situations if it is used as a measure of
structural response rather than as a measure of the input force.
Several gages, each with a different natural frequency, will yield
information which can at least be qualitatively interpreted as the
response of the structure in the frequency domain. This is basi-
cally the meaning of a shock spectrum.

40

Table V. Characteristics of Copper Ball Accelerometers

ADVANTAGES

- (1) Capable of sensing large g's

- (2) Reliable in use

- (3) Self-contained

- (4) Inexpensive to build and use

DISADVANTAGES

- (1) Nonlinear calibration curve

- (2) Copper-ball deformation is rate sensitive

- (3) Different deformation caused by dynamic and static calibration

- (4) Can deform cumulatively

- (5) May be more than a one degree of freedom system.

41

REFERENCES

(1) H. R. Kollmeyer, "Light gas gun for production of shock pressure in solids," HDL Report No. TR-933(1961).

(2) V. F. DeVost, "NOL copper ball accelerometers," U.S. Naval Ordnance Laboratory, White Oak, Md. NAVORD Report 6925(1960).

(3) W. Goldsmith, "Impact," Edward Arnold, Ltd., London, 1960.

(4) W. Herrman and A. H. Jones, "Survey of hypervelocity impact information," Mass. Inst. of Tech., Aeroelastic and Structures Res. Lab. Report 99-1(1961).

(5) W. A. Allen et al, "Dynamics of projectile penetrating sand," J. Appl. Phys. 28,370(1957).

(6) F. F. Vitman and N. A. Zlatin, "Collision of deformable bodies and its modeling I. Status and theory of the problem," Soviet Physics - Technical Physics 8, 730(1964).

(7) J. L. McCarty and H. D. Carden, "Impact characteristics of various materials obtained by acceleration-time-history technique applicable to evaluating remote targets," NASA-TN-D-1269(1962).

(8) P. A. Brody, "Strong shock waves in polled barium titanate ceramic elements," Diamond Ordnance Fuze Laboratories Report TR-869 (1960).

(9) H. Hilliar, "Experiments on the pressure wave thrown out by submarine explosions," Underwater Explosion Research, Vol. 1, U.S. Government Printing Office, Washington, D. C.

(10) A. B. Arons, "Response of the ball crusher gauge to various driving functions," paper in "Underwater explosion Research," Vol. 1, U. S. Government Printing Office, Washington, D. C.

(11) G. Chertock, "The response of a ball crusher gage," David Taylor Model Basin Report 751(1951).

(12) R. H. Cole, "Underwater explosions," Princeton Univ. Press, Princeton, N. J., (1948).

(13) Anon, "Weapon pressure instrumentation," U.S. Army Test and Evaluation Command, Aberdeen Proving Ground, Material Test Procedure 3-2-810(1966).

Preceding Page Blank

REFEREN ~S 'Cont'd)

(14) H. J. Davis, "Notes on the use of shock spectra in the
shock testing of artillery fuze and fuze components," HDL Technical
Memorandum (in preparation).

(15) J. L. Rand, "Dynamic compression testing of crusher gage
material," U. S. Naval Ordnance Laboratories, White Oak, Md., NOL-
TR-63-277(1964).

(16) H. M. Cole, "An investigation of the dynamic deformation
of small copper balls," U. S. Naval Ordnance Laboratories, White Oak,
Md.

(17) J. Corner, "Theory of the interior ballistics of guns,"
J. Wiley & Sons, New York (1950).

(18) J. R. Vigliante, "Dynamic calibration of spherical copper
crushers," Aberdeen Proving Ground Development and Proof Services
Report 1045, Nov 1963.

(19) J. L. McCarty and J. Pearson, "Study of dynamic response
to impact loadings of acceleration sensors having various mounting
characteristics," NASA Technical Note TND-3973(May 1967).

DOCUMENT CONTROL DATA - R & D

Security classification of title, body of abstract and indexing annotation must be entered when the overall report is classified,

1 ORIGINATING ACTIVITY *(Corporate author)*	2a. REPORT SECURITY CLASSIFICATION
Harry Diamond Laboratories Washington, D. C. 20438	UNCLASSIFIED
	2b. GROUP

3 REPORT TITLE

IMPACT TESTING WITH A FOUR-INCH AIR GUN AND LEAD TARGETS

4 DESCRIPTIVE NOTES *(Type of report and inclusive dates)*

5 AUTHOR(S) *(First name, middle initial, last name)*

Harry J. Davis

6 REPORT DATE	7a. TOTAL NO OF PAGES	7b. NO. OF REFS
April 1968	52	19

8a. CONTRACT OR GRANT NO	9a. ORIGINATOR'S REPORT NUMBER(S)
b. PROJECT NO DA-1N523801A301	TR-1383
c. AMCMS Code: 5523.11.62500	9b. OTHER REPORT NO(S) *(Any other numbers that may be assigned this report)*
HDL Proj. No. 36500 d.	

10 DISTRIBUTION STATEMENT

This document has been approved for public release and sale; its distribution is unlimited.

11 SUPPLEMENTARY NOTES	12. SPONSORING MILITARY ACTIVITY
	AMC

13 ABSTRACT

This report evaluates an HDL method of testing fuzes and fuze components for ruggedness. The test items are mounted in projectiles and fired from an air gun into 3- to 10-in. thick lead blocks. The projectile deceleration upon striking this target provides the test. The evaluation is based on 3 years of routine test data.

The measured quantity of primary interest is the peak acceleration obtained from copper ball accelerometers. These measurements indicate that structures or components with natural frequencies of hundreds of Hertz experience peak accelerations of 5000 to 50,000 g. Hundreds of thousands of g's, however, have been measured at natural frequencies greater than 10 kHz. Such measurements may differ by factors of two at different points within the projectile.

This report presents a brief description of the air-gun design and test techniques, the advantages and disadvantages of using the copper ball accelerometers for these measurements, and the target penetration phenomena since they provide the force pulses experienced by the projectile. The usual constant retarding force law and the Poncelet solid penetration law are applied in this study.

DD FORM 1473 REPLACES DD FORM 1473, 1 JAN 64, WHICH IS OBSOLETE FOR ARMY USE.

UNCLASSIFIED
Security Classification

51

t4 KEY WORDS	LINK A		LINK B		LINK C	
	ROLE	WT	ROLE	WT	ROLE	WT
1. Accelerometers						
2. Penetration phenomena						
3. Shell response						
4. Impact testing						
5. Shock testing						
6. Air guns						

GPO 941-282